Journal of Medicinal Chemistry

Article

pubs.acs.org/jmc

Optimization of a Small Tropomyosin-Related Kinase B (TrkB) Agonist 7,8-Dihydroxyflavone Active in Mouse Models of Depression

Xia Liu,[†] Chi-Bun Chan,[†] Qi Qi,[†] Ge Xiao,[‡] Hongbo R. Luo,[§] Xiaolin He,[∥] and Keqiang Ye*[,†]

[†]Department of Pathology and Laboratory Medicine, Emory University School of Medicine, 615 Michael Street, Atlanta, Georgia 30322, United States

[‡]Centers for Disease Control and Prevention, 4770 Buford Highway, Atlanta, Georgia 30341, United States

[§]Department of Pathology and Lab Medicine, Harvard Medical School and Children's Hospital Boston, 10214 Karp Research Building, 1 Blackfan Circle, Boston, Massachusetts 02115, United States

[∥]Department of Molecular Pharmacology and Biological Chemistry, Northwestern University Feinberg School of Medicine, 303 E. Chicago Avenue, Searle 8-417, Chicago, Illinois 60611, United States

Supporting Information

ABSTRACT: Structure–activity relationship study shows that the catechol group in 7,8-dihydroxyflavone, a selective small TrkB receptor agonist, is critical for agonistic activity. To improve the poor pharmacokinetic profiles intrinsic to catechol-containing molecules and to elevate the agonistic effect of the lead compound, we initiated the lead optimization campaign by synthesizing various bioisosteric derivatives. Here we show that the optimized 2-methyl-8-(4′-(pyrrolidin-1-yl)phenyl)chromeno[7,8-*d*]imidazol-6(1*H*)-one derivative possesses enhanced TrkB stimulatory activity. Chronic oral administration of this compound significantly reduces the immobility in forced swim test and tail suspension test, two classical antidepressant behavioral animal models, which is accompanied by robust TrkB activation in hippocampus of mouse brain. Further, in vitro ADMET studies demonstrate that this compound possesses the improved features compared to the previous lead compound. Hence, this optimized compound may act as a promising lead candidate for in-depth drug development for treating various neurological disorders including depression.

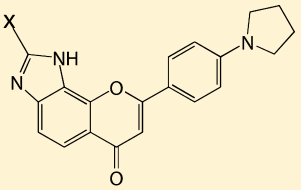

X: H; CH3

INTRODUCTION

Brain-derived neurotrophic factor (BDNF) is a member of the neurotrophin family, which includes nerve growth factor (NGF), NT-3, and NT-4/5. BDNF binding to its cognate receptor, TrkB, triggers its dimerization through conformational changes and autophosphorylation of tyrosine residues, resulting in activation of the three major signaling pathways, MAPK, PI3K, and PLC-γ.[1] Accumulating evidence indicates that these molecules are also critical for antidepressant drug efficacy. Antidepressants induce BDNF mRNA expression, as well as autophosphorylation and activation of TrkB,[1,2] and the behavioral effects of antidepressants in the forced swim test are attenuated in mice with only one active BDNF allele (BDNF$^{\pm}$ mice), completely lacking BDNF specifically in forebrain or expressing a dominant negative form of TrkB (trkB.T1).[2,3] Ablation of TrkB, specifically in hippocampal neuronal progenitor cells renders the mice behaviorally nonresponsive to chronic antidepressant treatment.[4] Hence, these results suggest a model whereby chronic antidepressant treatment induces BDNF expression and long-term activation of TrkB, leading to an antidepressant effect.[5−7]

The preclinical evidence strongly supports the idea that BDNF might be useful as a therapeutic agent for a variety of neurological disorders.[8,9] To search for small molecules that mimic the biological functions of BDNF, we invented a cell-based assay and identified two small molecular TrkB agonists with different structural backbones.[10,11] Our studies demonstrate that these small molecules exert potent neuroprotective effects in stroke and PD and possess robust antidepressant effect.[10,12] Both 7,8-dihydroxyflavone (7,8-DHF)[10,12] and deoxygedunin induce neurogenesis and exhibit antidepressant-like profile in a TrkB-dependent manner.[11,12] Most recently, it has been shown that 7,8-DHF mimics BDNF and improves the cognitive defect in AD.[13] Further, 7,8-DHF dampens the development of the "depressive" phenotype.[14] Like BDNF, 7,8-DHF rescues synaptic plasticity in aged animals.[15] Notably, 7,8-DHF exhibits therapeutic efficacy in a mouse model of Rett syndrome, caused by mutations in the MeCP2 gene; MeCP2 mutant mice have reduced levels of BDNF.[16] Hence, these studies demonstrate that our small TrkB agonists mimic BDNF and exert neuroprotective roles in various neurological diseases and display an antidepressant-like profile.

Our preliminary structure–activity relationship (SAR) study shows that the 7,8-dihydroxy groups are essential for the agonistic effect.[12] To improve the lead compound's agonistic activity, we have conducted an extensive SAR study and synthesized numerous derivatives. We have successfully identified 4′-dimethylamino-7,8-dihydroxyflavone (4′-DMA-7,8-DHF)[12] that displays higher TrkB agonistic activity than

Received: July 26, 2012
Published: September 17, 2012

   dx.doi.org/10.1021/jm301099x | *J. Med. Chem.* 2012, 55, 8524–8537

Table 1. In Vivo Pharmacokinetic Studies[a]

compd	route of administration	dose (mg/kg)	subject	$t_{1/2}$ (min)	CL (mL min^{-1} kg^{-1})	V_z (mL/kg)	V_{ss} (mL/kg)	AUC_{last} (min·ng/mL)	AUC_{INF} (min·ng/mL)
4′-dimethylamino-7,8-dihydroxflavone HBr	iv	1	mice	9	168	2117	803	5930	5943
13	iv	3	mice	103	156	23085	10011	18746	19229
compd	route of administration	dose (mg/kg)	subject	bioavailability (%)	T_{max} (min)	C_{max} (ng/mL)	$t_{1/2}$ (min)	AUC_{last} (min·ng/mL)	AUC_{INF} (min·ng/mL)
4′-dimethylamino-7,8-dihydroxflavone HBr	po	5	mice	NC	NC	NC	NC	NC	NC
13	po	10	mice	2	120	7	58	1144	1293

[a]Pharmacokinetic parameters were derived from a noncompartmental model using WinNonlin 5.2. $t_{1/2}$ = elimination half-life. CL = total body clearance. V_z = volume of distribution. V_{ss} = an estimate of the volume of distribution at steady state. AUC_{last} = area under the concentration−time curve from the time of dosing to the time of last observation that is greater than the limit of quantitation. AUC_{INF} = area under the concentration−time curve from the time of dosing, extrapolated to infinity. Linear/log trapezoidal method was used for AUC_{last} and AUC_{INF} calculations. T_{max} = time of maximum observed concentration. C_{max} = concentration corresponding to T_{max}. NC = not calculable because plasma concentrations are too low.

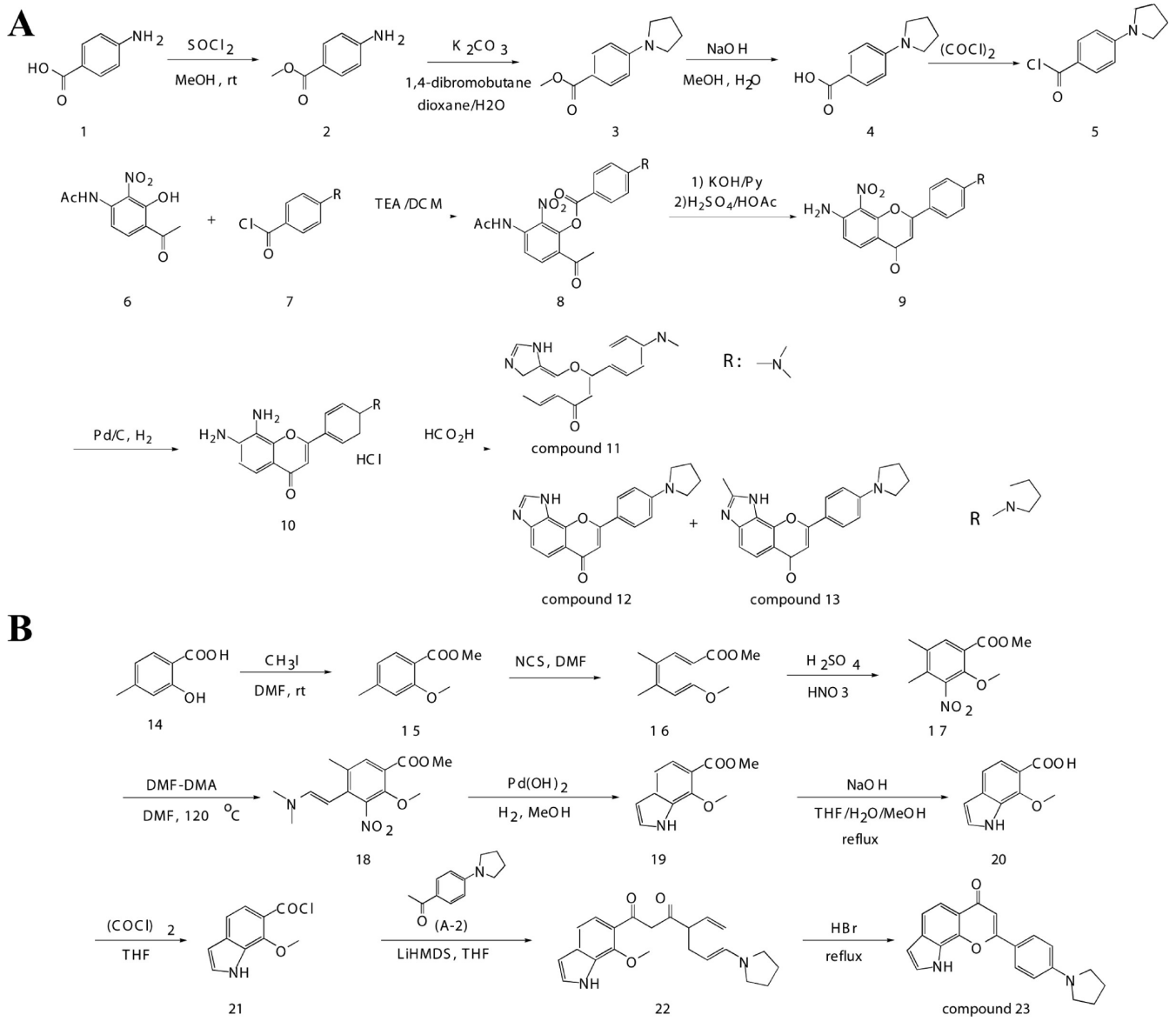

Figure 1. Organic synthesis of various flavonoids. (A) Schematic diagram of synthetic routes for 4′-dimethylamino-7,8-imidazoleflavone (compounds **11**, **12**, and **13**). R represents dimethylamino group or 4-pyrrolidin-1-yl-group. (B) Schematic diagram of synthetic route for compound **23**.

the original hit 7,8-DHF. This novel compound also exhibits a more robust and longer TrkB activation effect in animals. Consequently, this new compound reveals more potent antiapoptotic activity. Interestingly, chronic oral administration of 4′-DMA-7,8-DHF and the original hit 7,8-DHF strongly promotes neurogenesis in dentate gyrus and demonstrates

dx.doi.org/10.1021/jm301099x | J. Med. Chem. 2012, 55, 8524−8537

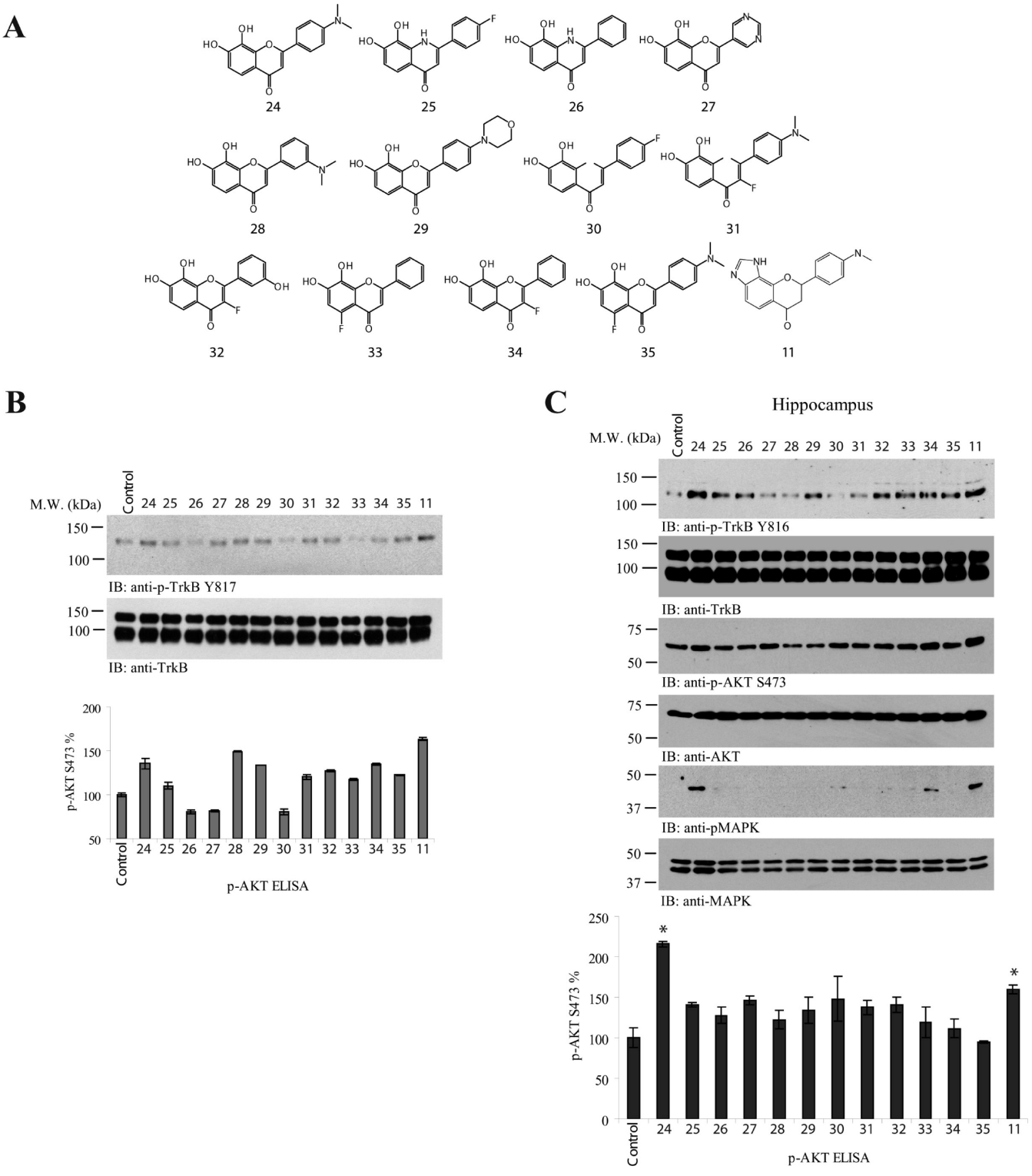

Figure 2. 8-(4-(Dimethylamino)phenyl)chromeno[7,8-*d*]imidazol-6(1*H*)-one exhibits elevated TrkB stimulatory activity. (A) Chemical structures of various synthetic flavonoids. (B) 8-(4-(Dimethylamino)phenyl)chromeno[7,8-*d*]imidazol-6(1*H*)-one displays stronger TrkB stimulatory activity than the lead compound **24**. Primary cortical cultures from E17 rat embryos were treated with 500 nM various synthetic flavone derivatives for 15 min. The cell lysates (20 μg) were analyzed by p-TrkB immunoblotting (top panel) and p-Akt ELISA (bottom panel). The data were from two sets of replicated experiments (mean ± SEM). (C) 8-(4-(Dimethylamino)phenyl)chromeno[7,8-*d*]imidazol-6(1*H*)-one strongly activates TrkB receptor in mouse brain. Various indicated compounds at 1 mg/kg were orally administrated into C57 BL/6J mice, and TrkB phosphorylation and its downstream signaling cascades including Akt and MAPK in the hippocampus of mouse brain were analyzed by immunoblotting at 4 h. Compounds **11** and **24** displayed the strongest TrkB stimulatory effect (first panel). The downstream p-Akt and p-MAPK activity coupled to the TrkB activation patterns (third and fifth panels). p-Akt 473 ELISA results of drug treated mouse brain were analyzed (seventh panel) (∗, $P < 0.05$ vs control; one-way ANOVA). The data were from two sets of replicated experiments (mean ± SEM).

dx.doi.org/10.1021/jm301099x | *J. Med. Chem.* 2012, 55, 8524−8537

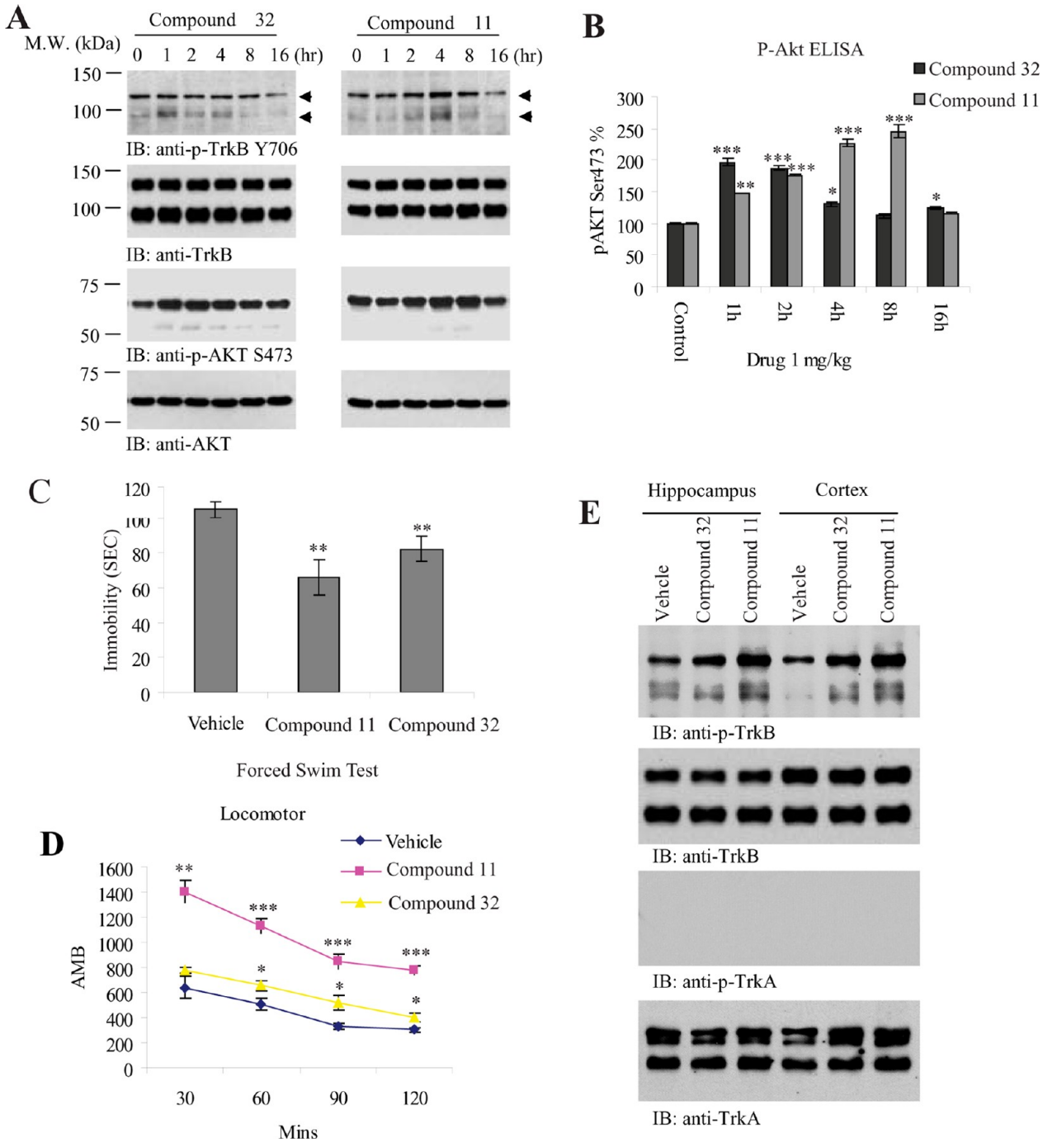

Figure 3. 8-(4-(Dimethylamino)phenyl)chromeno[7,8-*d*]imidazol-6(1*H*)-one strongly activates TrkB and reduces the immobility in forced swim test. (A) Time course assay of 8-(4-(dimethylamino)phenyl)chromeno[7,8-*d*]imidazol-6(1*H*)-one. Compound (**32**) and compound (**11**) at 1 mg/kg were orally administrated into C57 BL/6J mice, and TrkB phosphorylation and its downstream signaling cascades including Akt in mouse brain were analyzed by immunoblotting at various time points. TrkB activation by compound **11** peaked at 4 h, whereas the maximal TrkB activation by compound **32** in mouse brain occurred at 1−2 h. Arrows indicate the p-TrkB in mature glycosylated or unglycosylated forms (first panels). The downstream Akt activation pattern tightly correlated with the upstream TrkB activation (third panels). (B) p-Akt S473 in drug-treated mouse brain was by ELISA using 20 μg of brain lysates (∗, $P < 0.05$; ∗∗, $P < 0.01$; ∗∗∗, $P < 0.001$ vs control; one-way ANOVA). The data were from two sets of replicated experiments (mean ± SEM). (C) Forced swim test with compounds **11** and **32**. The test (6 min, immobility recorded in the last 4 min) was performed with male C57BL/6J mice that have been orally administrated 5 mg/kg compound **11**, compound **32**, or vehicle solvent saline for 21 days. Data are presented as the mean ± SEM ($n = 6$, ∗∗, $P < 0.01$ vs vehicle, Student t test). (D) Locomotor activity assay. Drug-treated mice as stated in (C) were tested for locomotor activity at day 22. Compound **11** but not **32** significantly increased the locomotor activity compared to vehicle control. Data are presented as the mean ± SEM ($n = 6$; ∗, $P < 0.05$; ∗∗∗, $P < 0.001$; two-way ANOVA). (E) TrkB but not TrkA is activated by compounds **11** and **32** in mouse brain. The brain lysates from chronic drug-treated mice were analyzed by immunoblotting with anti-p-TrkA 794 and p-TrkB 816.

dx.doi.org/10.1021/jm301099x | *J. Med. Chem.* 2012, 55, 8524−8537

marked antidepressant-like profile.[12] However, catechol containing compounds usually have short in vivo half-lives and are prone to be cleared in the circulatory system following oxidation, glucuronidation, sulfation, or methylation.[17,18] The potential metabolic pathways implicated in catechol-containing 7,8-DHF clearance in the circulatory system may remain similar. To overcome the intrinsic pharmacokinetics (PK) shortcomings that catechol groups are associated with, we replaced 7,8-dihydroxy groups with an imidazole ring. In this report, we expand on our previous findings to include the synthesis of numerous imidazole-substituted flavonoids with improved in vitro ADMET profiles, efficacy in activating the TrkB receptor in mouse brain, and elevated antidepressant effects.

RESULTS

Synthesis of Imidazole Flavonoid and Indole Flavonoid Derivatives. Previous study shows that the catechol group plays a critical role in regulating 7,8-DHF and its derivatives' TrkB agonistic effect. Since catechol-containing compounds usually possess relatively poor PK profiles, we synthesized numerous analogues of this compound to enhance the desired biological and physical properties of the lead compound 4′-DMA-7,8-DHF. The in vivo PK data for this compound are included in Table 1. To synthesize the intermediate 4-dimethylaminobenzoyl chloride or 4-pyrrolidin-1-ylbenzoyl chloride, we conducted the reactions described in the top of Figure 1A. 4-(Dimethylamino)benzoyl chloride (**7**, R = dimethylamino) was coupled to *N*-(4-acetyl-3-hydroxy-2-nitrophenyl)acetamide (**6**) in the presence of triethylamine to yield 3-acetamido-6-acetyl-2-nitrophenyl 4-(dimethylamino)-benzoate (**8**), which was subsequently cyclized to afford 7-amino-2-(4-(dimethylamino)phenyl)-8-nitro-4*H*-chromen-4-one (**9**). This compound was reduced to generate 7,8-diamino-2-(4-(dimethylamino)phenyl)-4*H*-chromen-4-one hydrochloride (**10**). A solution of this compound was refluxed in HCO_2H for 1 h to produce a yellow solid, which was recrystallized to yield pure 8-(4′-(dimethylamino)phenyl)-chromeno[7,8-*d*]imidazol-6(1*H*)-one (compound **11**). The 4′-pyrrolidinoimidazole derivatives were synthesized with similar routes, producing a mixture of imidazole flavonoid (compound **12**) and methylimidazole flavonoid (compound **13**) with 60:40 ratio (Figure 1A), which was separated with pre-HPLC to give compound **12** as an orange solid and a dark-yellow solid compound **13**. The yield for the 2-methylimidazole side product in 4′-dimethylamino derivative was very low compared to that for compound **11**. For compound **12**, 16 hydrogen atoms were present in the ^{1}H NMR, while for compound **13**, 18 protons appeared. We reasoned that the methyl group was on the imidazole ring because the proton between the two nitrogen atoms of the imidazole ring was missing (8.81 ppm in compound **12**) and the chemical shift of methyl group was consistent with the structure. To prepare the intermediate 7-methoxy-6-indolecarboxylic chloride (**21**), we employed compound **14** as a starting material, via the reactions described in the top of Figure 1B. The obtained intermediate compound **21** was then coupled to 4′-pyrrolidinophenyl methyl ketone in the presence of LiHMDS, and the reaction mixture was quenched with NH_4Cl water solution to give compound **22** (1-(4′-pyrrolidinophenyl)-3-(7′-methoxy-6-indolyl)propane-1,3-dione), which was subsequently cyclized in the presence of HBr to afford compound **23** (Figure 1B). The yield for each step in the synthesis is indicated in the Experimental Procedures.

8-(4′-(Dimethylamino)phenyl)chromeno[7,8-*d*]-imidazol-6(1*H*)-one Displays Increased TrkB Stimulatory Effect. Our previous study shows that the electron donor dimethylamino group at the 4′ position of the B ring significantly elevates the agonistic effect.[12] Hence, we wanted to test the 3′-dimethylamino or the 4′-morpholino group's effect on 7,8-DHF's TrkB agonistic activity. Further, we wondered about the effect of the electron-withdrawing group, fluoro, on 7,8-DHF or 4′-DMA-7,8-DHF's agonistic activity (Figure 2A). To compare the TrkB activation by these compounds, we prepared primary cortical cultures and treated them with 500 nM various compounds for 15 min and collected the cell lysates. Compound **11** exhibited a stronger effect in triggering TrkB activation than the lead compound 4′-DMA-7,8-DHF (**24** in Figure 2A). 3′-Dimethylamino-7,8-DHF (**28**) or 4′-morpholino-7,8-DHF (**29**) exhibited activity comparable to that of the lead compound **24**. Fluoride substitution at position 3 or 5 (**32**, **33**, **34**, and **35**) did not significantly affect 7,8-DHF's TrkB agonistic activity. Fluoride substitution at the 4′ position on the B ring (**30**) inhibited its activity, which might be due to its electron-withdrawing effect. As we showed before,[12] replacing an O atom with an N atom in the C ring (compounds **25** and **26**) diminished agonistic activity (Figure 2B, upper panel). The p-Akt ELISA results were similar to the TrkB activation pattern (Figure 2B, lower panel). To further explore these compounds' effects on TrkB activation in mouse brain, we orally administrated 1 mg/kg each compound and monitored TrkB's activity at 4 h. As expected, the lead compound **24** clearly activated the TrkB receptor; 4′-dimethylamino-7,8-imidazoleflavone (**11**) also robustly activated TrkB. The rest of the compounds displayed a similar effect, as was observed by the in vitro assay (Figure 2C, top panel). Accordingly, the downstream p-Akt and p-MAPK signalings were activated by both compounds **24** and **11**. p-Akt ELISA analysis also correlated with the observations of p-TrkB immunoblotting (Figure 2C, bottom panel).

8-(4′-(Dimethylamino)phenyl)chromeno[7,8-*d*]-imidazol-6(1*H*)-one Is Active in Mouse Models of Depression with Increased Locomoter Activity. To gain insight into TrkB activation kinetics, 8-(4′-(dimethylamino)-phenyl)chromeno[7,8-*d*]imidazol-6(1*H*)-one (**11**) was administered to C57BL6 mice at 1 mg/kg via oral gavage. For comparison, we employed compound **32** in the same procedure. The mouse brains were collected, and TrkB activation and its downstream Akt signaling were analyzed by immunoblotting. Compound **11** activated TrkB receptor in a time-dependent manner, peaking at 4 h and fading away at 16 h. The p-Akt signal was in alignment with the upstream p-TrkB activity. Compound **32** displayed less effect on TrkB activation than compound **11** (Figure 3A, top and third panels). P-Akt ELISA correlated with p-Akt immunoblotting results for both compounds. Compound **11** gradually activated Akt and climaxed at 8 h, where the p-Akt signal was elevated by about 250% compared to the control. Compound **32** also elicited p-Akt activation peaking at 1 h, declining at 4 h, and returning to the baseline at 8 h. The peak magnitude of Akt activation by compound **32** was significantly less than that by compound **11** (Figure 3B). Forced swim test (FST) is broadly used for screening potential antidepressant drugs and is widely used to measure antidepressant activity. The FST is a good screening tool with good reliability and predictive validity.[19,20]

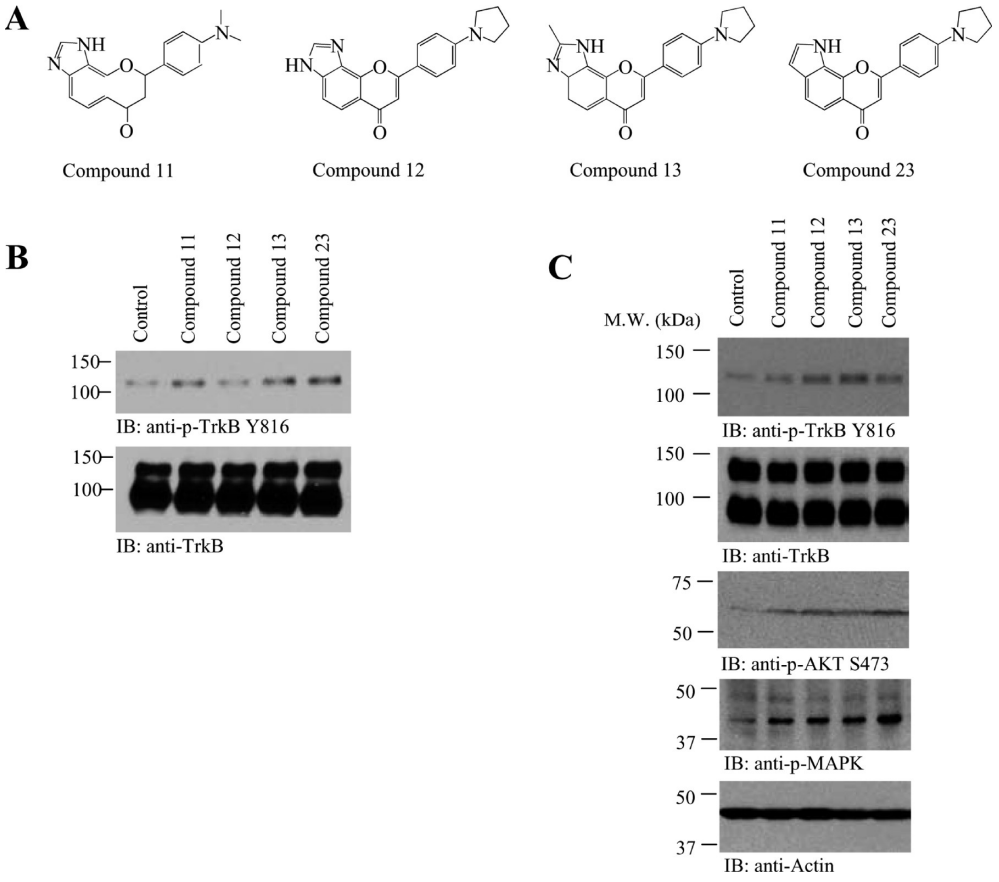

Figure 4. 2-Methyl-8-(4-(pyrrolidin-1-yl)phenyl)chromeno[7,8-*d*]imidazol-6(1*H*)-one (compound **13**) triggers TrkB activation in primary neurons and mouse brain. (A) Chemical structures of various synthetic 4′-pyrrolidinoflavone derivatives. (B) 2-Methyl-8-(4-(pyrrolidin-1-yl)phenyl)-chromeno[7,8-*d*]imidazol-6(1*H*)-one (compound **13**) triggers TrkB activation in primary neurons. Rat primary neurons were treated with 500 nM various compounds for 15 min. Cell lysates (20 mg) were analyzed with various antibodies as indicated. (C) 2-Methyl-8-(4-(pyrrolidin-1-yl)phenyl)chromeno[7,8-*d*]imidazol-6(1*H*)-one (compound **13**) triggers TrkB activation in mouse brain. Various compounds at 1 mg/kg were orally administrated into C57 BL/6J mice, and TrkB phosphorylation (first panel) and its downstream signaling cascades including Akt and MAPK in the hippocampus of mouse brain were analyzed by immunoblotting at 2 h. The downstream p-Akt and p-MAPK activity were coupled to the TrkB activation patterns (third and fourth panels).

To explore whether these compounds possess any antidepressant effect, we chronically treated C57/BL6 J mice with 5 mg/kg compound, once a day for 3 weeks. At the end of the treatment, we conducted the locomoter activity assay, followed by a forced swim test. We found that both compounds significantly reduced the immobility and the effect of compound **11** was more robust than that of compound **32** (Figure 3C). Nonetheless, compound **11** substantially augmented locomoter activity compared to compound **32** and vehicle control (Figure 3D). Immunoblotting with brain tissues from both cortex and hippocampus demonstrated that both compounds **11** and **32** clearly escalated TrkB phosphorylation after 3 weeks of drug treatment compared to vehicle control but compound **11** displayed a stronger effect than compound **32**. The TrkA receptor was not activated by any of these compounds (Figure 3E), demonstrating that they are TrkB receptor-specific agonists.

2-Methyl-8-(4′-(pyrrolidin-1-yl)phenyl)chromeno[7,8-*d*]imidazol-6(1*H*)-one Demonstrates Greater Potency than 8-(4′-(Dimethylamino)phenyl)chromeno[7,8-*d*]-imidazol-6(1*H*)-one. Though compound **11** possessed robust TrkB stimulatory effect and reduces immobility in forced swim test, it escalated locomotor activity after 3 weeks of administration. To alleviate this concern, we synthesized several imidazole or indole-substituted flavonoid compounds (Figure 4A). Immunoblotting and p-Akt ELISA analysis demonstrated that both compounds **13** and **23** displayed higher activity than compound **11** in triggering TrkB and Akt activation in primary neurons (Figure 4B). We made similar observations about TrkB receptor and Akt activation in mouse brain 2 h after oral administration of 1 mg/kg compounds (Figure 4C). Hence, we chose to focus on compounds **13** and **23** to examine their antidepressant effect in both forced swim test and tail suspension test assays.

2-Methyl-8-(4′-(pyrrolidin-1-yl)phenyl)chromeno[7,8-*d*]imidazol-6(1*H*)-one Demonstrates Antidepressant-like Profile without Altering Locomoter Activity. Next, we treated the mice with compounds **13** and **23** at a dosage of 2.5 mg/kg via oral gavage once a day for 3 weeks and to explore their effect on locomotor activity. FST showed that compound **13** significantly reduced the immobility by 45% compared to vehicle control; by contrast, compound **23** had no effect (Figure 5A). The tail suspension test (TST) has become one of the most widely used models for assessing antidepressant-like activity in mice. The test is based on the fact that animals subjected to the short-term, inescapable stress of being suspended by their tail will develop an immobile posture. Various antidepressant medications reverse the immobility and

dx.doi.org/10.1021/jm301099x | *J. Med. Chem.* 2012, 55, 8524−8537

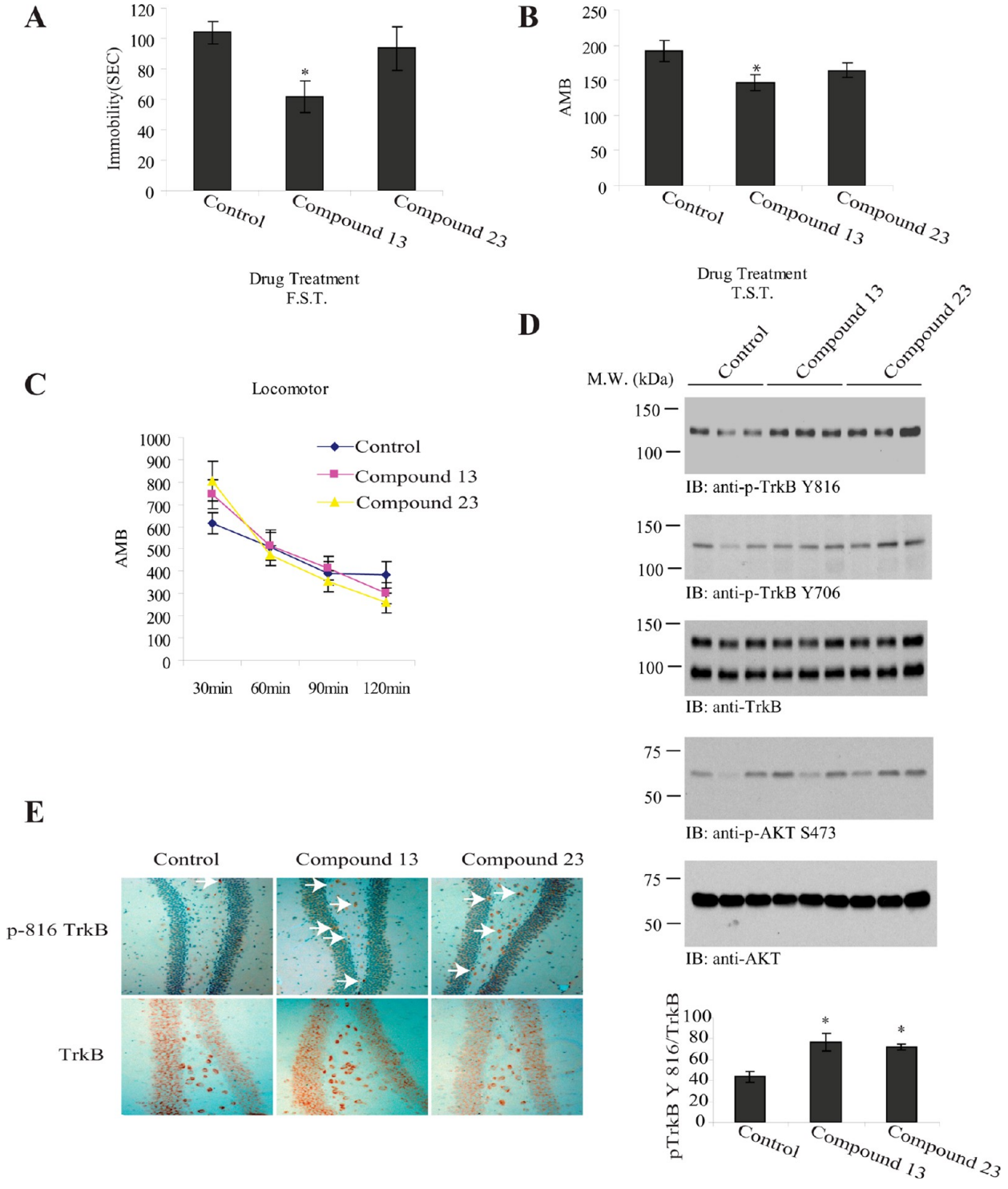

Figure 5. 2-Methyl-8-(4-(pyrrolidin-1-yl)phenyl)chromeno[7,8-*d*]imidazol-6(1*H*)-one (compound **13**) triggers TrkB activation in mouse brain and exhibits antidepressant effect. (A) Forced swim test (6 min, immobility recorded in the last 4 min) was performed with male C57BL/6J mice that have been orally administrated 2.5 mg/kg **13**, **23**, or vehicle solvent saline for **21**. Compound **13** but not compound **23** significantly decreased the immobility. Data are presented as the mean ± SEM (n = 8; ∗, $P < 0.05$; Student's t test). (B) Tail suspension test. The drug-treated mice were subjected to tail suspension assay. Compound **13** but not **23** reduced the immobility. Data are presented as the mean ± SEM (n = 8; ∗, $P < 0.05$; Student's t test). (C) Locomotor activity assay. None of the tested compounds significantly altered the locomotor activity. (D) Both compounds **13** and **23** activate TrkB and its downstream signaling cascades. Various compounds at 2.5 mg/kg were orally administered into C57 BL/6J mice, and TrkB phosphorylation and its downstream effector Akt activation in the hippocampus were analyzed by immunoblotting after behavioral tests. Both compounds **13** and **23** elevated TrkB phosphorylation (first panel). The downstream p-Akt activity was also up-regulated by compounds **13** and **23** (fourth panel). The ratio P-TrkB/total TrkB in drug-treated mouse brain was analyzed (sixth panel). The data were from two sets of replicated experiments and are expressed as the mean ± SEM (∗, $P < 0.05$ vs control; Student's t test). (E) Both compounds **13** and **23** elevated TrkB phosphorylation in the hippocampus. The drugs in chronic drug-treated mice were perfused, and the brain sections were stained with anti-p-TrkB 816 and anti-TrkB antibodies. The p-TrkB activated neurons were labeled with white arrows.

dx.doi.org/10.1021/jm301099x | *J. Med. Chem.* 2012, 55, 8524−8537

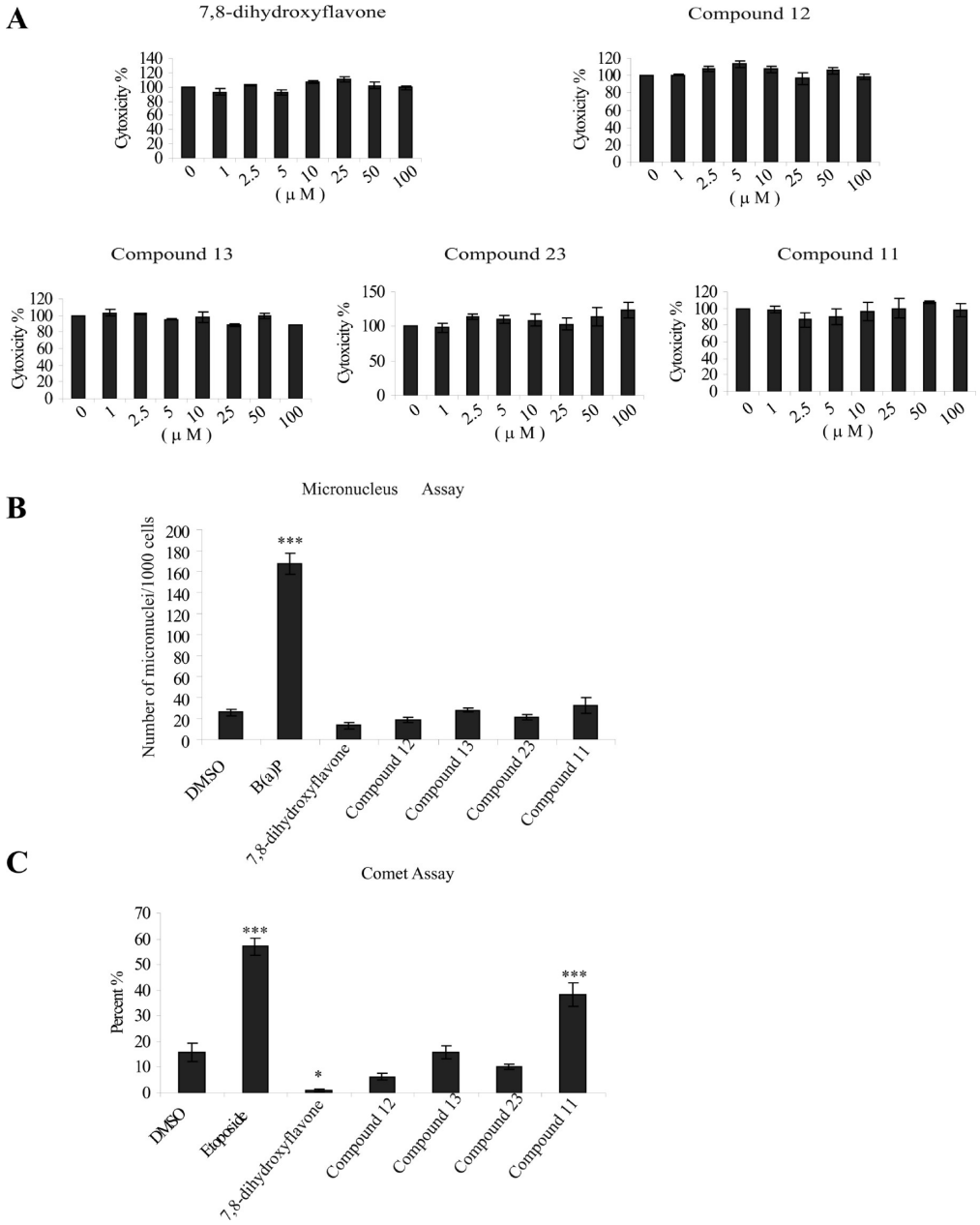

Figure 6. In vitro cytotoxicity and genotoxicity assay. (A) Cytotoxicity assay in hepatocyte HepG2 cells. HepG2 cells were treated with various concentrations of flavonoids for 24 h. The drug-treated cells were subjected LDH assay. Data are presented as the mean ± SEM (n = 3). (B) Micronuclei assay in hepatocyte HepG2 cells. HepG2 cells were treated with 50 μM various compounds for 24 h. The nuclei were stained with DAPI and analyzed under a fluorescent microscope. Data are presented as the mean ± SEM (n = 3; ***, P < 0.001 vs vehicle; one-way ANOVA). (C) Comet assays. HepG2 cells were treated with 100 μM various compounds for 24 h. The percentage of lesion DNA in tail was used as a parameter for measurement of DNA damage. Data are presented as the mean ± SEM (n = 3; ***, P < 0.001 vs vehicle; one-way ANOVA).

promote an escape-related behavior.[21] We made similar observations of compound **13** significantly reducing the immobility versus vehicle control, whereas compound **23** lacked efficacy (Figure 5B). Further, locomotor activity analysis revealed that neither compound **13** nor **23** altered the motion activity compared to vehicle control (Figure 5C). Immunoblotting using both anti-p-TrkB Y816 and anti-p-TrkB Y706 antibodies with brain tissues demonstrated that both compounds **13** and **23** markedly activated TrkB. P-Akt immunoblotting also correlated with the upstream TrkB activation (Figure 5D, top, second and fourth panels). Quantitative p-Akt ELISA assay supported that both compounds notably activated Akt, fitting with the observations by Western blotting (Figure 5D, bottom panel). Immunohistochemistry staining with anti-p-TrkB demonstrated that TrkB was activated by these two chemicals in dentate gyrus after 3 weeks of treatment (Figure 5E, white arrows). Therefore, chronic treatment with compound **13** promotes TrkB activation in the hippocampus of mice and produces potent antidepressant-like profile.

In Vitro ADMET Profiles of the Imidazole Derivatives. 7,8-DHF and other flavonoids have recently been shown to possess impressive antigenotoxic effects against DNA lesions and micronuclei induced in human hepatocellular carcinoma cells, HepG2, by a potent mutagen and carcinogen benzo[a]-pyrene (B(a)P).[22] In order to gain insight into the liabilities of

dx.doi.org/10.1021/jm301099x | J. Med. Chem. 2012, 55, 8524−8537

the drug candidates, we examined their in vitro toxicity. An LDH cytotoxicity assay, using HepG2 cells treated with various compounds for 24 h, demonstrated that none of the tested compounds induced noticeable cytotoxicity even up to 100 μM, suggesting that these compounds do not trigger cell death even at very high concentrations (Figure 6A). Micronuclei formation is an important end point in genotoxicity study. To assess whether these synthetic compounds possess any potential carcinogenicity, we conducted the micronucleus assay by treating HepG2 cells with 50 μM various compounds for 24 h, followed by DAPI staining. Quantitative analysis revealed that none of the tested compounds exhibited significant effect, whereas the positive control B(a)P robustly induced micronuclei (Figure 6B). Next, we performed a Comet assay with 100 μM drug-treated HepG2 cells. As a positive control, we chose etoposide, a topoisomerase inhibitor, which causes DNA strand breaks. Interestingly, compound **11** but not other synthetic derivatives induced DNA lesions (Figure 6C). Hence, these toxicity experiments support that compounds **12**, **13**, and **23** possess negligible cytotoxicity or genotoxicity.

To explore these compounds' in vitro ADMET profiles, we conducted numerous in vitro assays. Human liver microsomal stability assay showed that after 1 h of incubation, compound **23** had 1.2% remaining whereas compound **13** had 25.4% unchanged, supporting that compound **13** is more metabolically stable than compound **23**. Reactive metabolic screening assays support that compound **13** is quite stable in vitro whereas compound **23** formed numerous adducts (Tables 2 and 3). CYP screen inhibition demonstrated that at 3 μM, CYP1A2 was inhibited about 27.3% by compound **13** whereas compound **23** inhibited 37.4%. At 30 μM, the inhibition patterns contained similar trends. The detailed inhibition data are summarized in Table 4. To test the possible cardiovascular toxicity, we examined hERG inhibition triggered by compound **13**. The hERG inhibition assay revealed that compound **13** did not possess any concentration-dependent inhibition activity of hERG. A human plasma protein binding experiment showed that both compounds **13** and **23** displayed approximately 99.9% of protein binding (Table 5). Hence, compound **13** possesses a much more preferable in vitro ADMET profile than compound **23**, fitting with its remarkable in vivo antidepressant efficacy.

Table 2. Summary of Microsomal Stability Screening

compd	test concn (μM)	test species	mean remaining parent with NADH (%)	mean remaining parent NADPH-free (%)
13	1	human	25.4	92.2
23	1	human	1.2	79.6

Table 3. Summary of Reactive Metabolite Identification

compd	scan	potential reactive metabolites identified	m/z	comment
13	precursor	no		no adduct detected
	neutral loss	no		
23	precursor	yes	627, 643	
	neutral loss	yes	605, 629, 659, 675	

Table 5. Summary of Plasma Protein Binding

compd	test concn (μM)	test species	Fu_{plasma} (%)	mean plasma fraction bound (%)	recovery (%)	binding classification
13	5	human	0.03	99.9	86.3	high binding
23	5	human	0.07	99.9	97	high binding

To investigate whether compound **13** possesses an improved in vivo PK profiles compared to the lead compound **24**, we conducted in vivo pharmacokinetic studies in mice. The PK parameters are summarized in Table 1. For the lead compound **24**, we employed the dosage of 1 mg/kg via iv injection and 5 mg/kg for the po route. At 1 mg/kg, the in vivo half-life, $t_{1/2}$, of the lead compound **24** in circulation was around 9 min and AUC_{last} was about 5930 (min·ng/mL), but the bioavailability of the lead compound **24** was not measurable at 5 mg/kg (Table 1). Thus, we increased the doses of the tested compound **13**. The $t_{1/2}$ for compound **13** was about 103 min with AUC_{last} of approximately 18 746 (min·ng/mL) at a dose of 3 mg/kg. Moreover, the bioavailability was around 2% at a 10 mg/kg dosage. Hence, these data demonstrate that compound **13** may possess an elevated PK profile compared to the lead compound **24**.

DISCUSSION

In the current report, we show that the synthetic 2-methyl-8-(4-(pyrrolidin-1-yl)phenyl)chromeno[7,8-*d*]imidazol-6(1*H*)-one (compound **13**) possesses improved in vitro ADMET features and is active in mouse models of depression. Moreover, in the mouse brain hippocampus, this compound activates the TrkB receptor and exerts robust antidepressant effects in both FST and TST assays. Therefore, our study demonstrates that this compound is a potential candidate for in-depth drug development. Molecular modeling also supports that 7,8-DHF and compound **13** might bind to the LRR motif on TrkB ECD (Supporting Information Figure 1), fitting with our previous results found with in vitro binding assay.[10,11] This approach may shed light on our future drug design for further improving the lead compound, if the cocrystal (agonist/TrkB ECD) structure is experimentally resolved.

Our previous structure–activity relationship (SAR) study demonstrates that the 7,8-dihydroxy groups on the A ring and the middle heteroatomic chromen-4-one C ring are essential for

Table 4. Summary of CYP Screening

compd	test concn (μM)	CYP3A4 modazolam (%)	CYP3A4 testoterone (%)	CYP2C9 (%)	CYP2C19 (%)	CYP2D6 (%)	CYP1A2 (%)
13	30	40.5	43.3	73.6	57.5	32.0	66.1
	3	10.8	4.5	12.4	11.1	8.7	27.3
23	30	48.1	18.7	52.9	90.0	81.6	75.9
	3	3.9	3.4	11.9	16.2	7.2	37.4

dx.doi.org/10.1021/jm301099x | J. Med. Chem. 2012, 55, 8524–8537

the TrkB stimulatory effect. Additionally, the 4′-position on the B ring is also critical for the agonistic effect. An electron-withdrawing group, such as F, or an electron-donating OH at this position suppresses the activity. Nonetheless, replacement with a dimethylamino or pyrrolidino group yields the desired activity. On the basis of the lead compound 4′-DMA-7,8-DHF, we initiated a lead optimization campaign by synthesizing a series of new compounds. Since the lead compound exhibits robust agonistic effect and potent antidepressant efficacy, we employed the bioisosteric strategy to enhance the desired biological or physical properties of a compound without making significant changes in chemical structure. We added a fluoride group at different positions and replaced the 7,8-dihydroxy groups with an imidazole ring or changed the dimethylamino group into a pyrrolidino ring. From compounds **31** and **32**, we found that addition of a fluoride group barely affects TrkB stimulatory activity (Figure 2). Replacing the 7,8-dihydroxy groups with an imidazole ring in compound **11** elevated its agonistic activity compared to the lead compound **24**, though the in vivo TrkB stimulatory activity remained comparable for these two compounds (Figure 2B,C). Although compound **11** strongly activated TrkB in mouse brain and decreased the immobility in FST, this compound highly augmented the locomotor activity as well (Figure 3), suggesting that it might reduce the immobility in FST by increasing the locomotor activity. Since the dimethylamino group may be prone to metabolic demethylation, we replaced the dimethylamino group with a pyrrolidino group. Remarkably, compound **13** not only displayed higher agonistic activity than compound **11** but also attenuated the locomotor enhancement effect by compound **11** (Figure 5). As expected, compound **13** was active in both FST and TST depression behavioral assays. It remains unclear why compound **23** exhibits potent TrkB stimulatory activity after oral administration but fails to show significant immobility reduction activity in either antidepressant behavioral assay. Conceivably, its high reactivity and poor microsomal stability account for its lack of an efficacious antidepressant effect (Tables 2 and 3).

Catechol-related compounds usually possess poor pharmacokinetic profiles because of oxidation, glucuronidation, sulfation, or methylation. For instance, catechol-containing apomorphine is a non-narcotic morphine derivative that acts as a potent dopaminergic agonist. Apomorphine metabolism occurs through several enzymatic pathways, including N-demethylation, sulfation, glucuronidation, and catechol O-methylation as well as nonenzymatic oxidation.[17] L-DOPA is the primary component of Parkinson's disease (PD) therapy; this drug is usually administered orally, but it is extensively metabolized in the gastrointestinal tract, so relatively little circulates in the bloodstream as intact L-DOPA. To minimize the conversion to dopamine outside the central nervous system, L-DOPA is usually given in combination with peripheral inhibitors of aromatic L-amino acid decarboxylase and COMT (catechol methyltransferase) inhibitor.[18] Our preliminary in vivo metabolism study shows that 7,8-DHF is also subjected to oxidation, glucuronidation, sulfation, and methylation (Supporting Information Figure 2). Among the modifications, glucuronidation and sulfation are mainly responsible for the in vivo clearance of the flavonoids. In addition, we have detected the O-methylated metabolites in both the plasma and brain samples after oral administration. Conceivably, these modification pathways may explain the relatively short half-lives of 7,8-DHF and its synthetic derivatives. Alteration of this labile group into the bioisosteric imidazole derivatives escalates the PK profile of compound **13** (Table 1). Though compound **13** displays an improved ADMET profile than the lead compound **24**, its oral bioavailability remains poor and the in vivo half-life is relatively short. Additional medicinal chemistry is needed to further optimize the lead compound and to improve the PK parameters.

Among the leading causes of drug candidate failure (~60%) are poor PK/ADME, toxicological properties, and adverse effects, which contribute more significantly than "lack of efficacy" (~30%). In order to optimize the ADME properties and also foresee liabilities of drug candidates, in vitro and in vivo ADMET (ADME plus toxicity) filters are being developed and implemented in various stages of the drug discovery and development process to alert to potential ADMET issues in the clinic.[23] Toxicology- and pharmacology-related safety has become a leading cause for compound failure during preclinical development and clinical trials. Most withdrawals of marketed drugs were associated with hERG inhibition[24,25] and hepatotoxicity.[26] Accordingly, we have examined our compounds' in vitro ADMET profiles. Remarkably, compounds **12**, **13**, and **23** exhibited negligible cytotoxicity or genotoxicity (Figure 6). The hERG inhibition index is also trifling for compound **13**. Moreover, the microsomal stability and reactive metabolic screening assays support that compound **13** is more stable than compound **23** in vitro. Though compound **13**'s in vivo half-life is about 103 min in mice, its oral bioavailability is only 2%. Nonetheless, it exhibited a much improved in vivo PK profile than the lead compound **24** (Table 1), demonstrating our progress in the optimization mission. It is worth noting that there is significant discrepancy between the remarkable therapeutic efficacy in the mouse models of antidepression and poor in vivo oral bioavailability. The potential explanation for this difference might be the compound's extreme potency so that a low concentration in the circulation system is sufficient for provoking the physiological effects. It is also possible that the metabolites of the compound are active as well. For instance, the B ring in compound **13** can be metabolized via hydroxylation in the lead compound **24** and compound **13**. Our previous study shows that hydroxylation on 2′ or 3′ position escalates 7,8-DHF's agonistic activity.[12] On the other hand, it remains unclear how 4′-DMA-7,8-DHF, which has a short half-life, exerts its physiological activities in animals. Conceivably, its O-methylated or B-ring hydroxylated metabolites in mouse brain might contribute to these actions. Clearly, further medicinal chemistry is necessary to continue developing compound **13** to meet the preclinical standards for a promising candidate. Specifically, we will determine the potential metabolites, which may shed light on how to metabolically stabilize this compound. Further, we will reduce the candidate's plasma protein binding affinity so that we can improve its brain bioavailability. Plausibly, the resynthesized novel compounds will possess longer $t_{1/2}$ and much-improved oral bioavailability with low toxicity. Together, our data support that 7,8-imidazole and 4′-pyrrolidone-substituted flavones are excellent lead compounds justifying further medicinal modification. These compounds not only provide a novel tool to dissect the biological functions of BDNF/TrkB signaling but also act as good lead compounds with great potential for future drug development for various neurological diseases, including depression.

EXPERIMENTAL PROCEDURES

Cells, Reagents, and Mice. Anti-p-TrkB 817 was from Epitomics. Anti-p-TrkB 706 was from Santa Cruz. Anti-TrkB antibody was from Cell Signaling. The wild-type C57BL/6 mice were bred in a pathogen-free environment in accordance with Emory Medical School guidelines. All chemicals not included above were purchased from Sigma. 7,8-DHF was purchased from TCI. The syntheses of compounds **24**–**27** were reported in our previous study.[12] The fluoro-substituted flavonoids in Figure 2A (compounds **25**, **30**, **31**, **32**, **33**, **34**, and **35**) were from Sundia (Shanghai, China). Compounds **28** and **29** in Figure 2A were provided by NIMH, Chemical Synthesis and Drug Supply Program at RTI. Experiments included NMR (Bruker AV300K, 300 MHz), MS (Shimadzu LCMS), and HPLC (PE, dual pumper, SPD detector, ODS-C18 reverse phase, 254 nm, CH_3CN–H_2O–0.1%TFA). Phospho-TrkB Y816 antibody was described before.[12] This phospho-TrkB was utilized for immunostaining the brain sections. Anti-TrkB (Cell Signaling, which recognizes both full-length and truncated TrkB) was used for immunoblotting. p-Akt 473 Sandwich ELISA was from Cell Signaling. BDNF was from Peprotech. Anti-phospho-TrkA 794, anti-TrkA, phospho-Akt-473, anti-Akt, and anti-phospho-Erk1/2 antibodies were from Cell Signaling.

Synthesis of Compounds 11, 12, 13, and 23. 4-Aminomethyl Benzoate (2). A solution of compound **1** (6.857 g, 50 mmol) in MeOH (120 mL) was treated with $SOCl_2$ (7 g, 59 mmol, 1.2 equiv) at −10 °C, and the mixture was stirred at room temperature overnight. LC–MS and TLC showed the reaction was over and the desired product was found. The mixture was concentrated and the residue was washed with Et_2O to give compound **2** as a pale-yellow solid (with purity of ∼95% by HPLC, 6.0 g, used for the next step without ^1H NMR confirmed).

Methyl 4-Pyrrolidin-1-ylbenzoate (3). A mixture of compound **2** (3.02 g, 20 mmol), K_2CO_3 (5.52 g, 40 mmol), and 1,4-dibromobutane (5.18 g, 24 mmol) in dioxane (30 mL) and water (30 mL) was treated with TBAB (*tert*-butylamine borane), and the mixture was refluxed for 48 h. LC–MS and TLC showed the reaction was not over and the desired product was found. The mixture was concentrated, and the residue was diluted with EA (ethyl acetate), washed with water and brine, and dried over Na_2SO_4. The mixture was concentrated and purified by silica gel (PE (petroleum ether) to PE/EA = 5:1 to 3:1) to give compound **3** as a pale-yellow solid (with purity of >95% by HPLC, 1.12 g, confirmed by ^1H NMR). ^1H NMR (400 MHz, DMSO-d_6): δ 7.82 (d, J = 8.8 Hz, 2H), 6.61 (d, J = 8.8 Hz, 2H), 3.81 (s, 3H), 3.36 (m, 4H), 2.02 (m, 4H).

4-(Pyrrolidin-1-yl)benzoic Acid (4). A mixture of compound **3** (1.12 g, 5.46 mmol) and NaOH (1.1 g, 27.3 mmol) in MeOH (15 mL) and water (15 mL) was refluxed overnight. LC–MS and TLC showed the reaction was over and the desired product was found. The mixture was concentrated and the residue was acidified with 6 N HCl to pH ≈ 3 and the precipitate was collected by filtration and dried with vacuum to give compound **4** as a white solid (with purity of >95% by HPLC, 600 mg, confirmed by ^1H NMR). ^1H NMR (400 MHz, DMSO-d_6): δ 12.03 (br s, 1H), 7.74 (d, J = 8.8 Hz, 2H), 6.54 (d, J = 8.4 Hz, 2H), 3.30 (m, 4H), 1.97 (m, 4H).

4-(Pyrrolidin-1-yl)benzoyl Chloride (5). To a suspension of compound **4** (115 mg, 0.6 mmol) in DCM (2 mL) at 0 °C was added DMF followed by $(COCl)_2$ (91 mg, 0.72 mmol). The mixture was stirred at room temperature for 2 h, and a clear solution was obtained. TLC (quenched by MeOH) showed the reaction was over. The mixture was concentrated, and to the residue was added toluene. Then the mixture was concentrated twice to give compound **5** as a pale-yellow solid, which was used for the next step without further purification.

8-(4′-(Dimethylamino)phenyl)chromeno[7,8-*d*]imidazol-6(1*H*)-one (11). 3-Acetamido-6-acetyl-2-nitrophenyl 4-(Dimethylamino)benzoate (8). To a mixture of *N*-(4-acetyl-3-hydroxy-2-nitrophenyl)acetamide (compound **6**, 1 g, 4.1 mmol, 1.0 equiv) and triethylamine (1.5 mL) was added 4-(dimethylamino)-benzoyl chloride (compound **7** with R = dimethylamino, 6.3 mmol) in three portions at 0 °C. Then the mixture was stirred at room temperature for 3 h. The mixture was diluted with dichloromethane (100 mL) and washed with 1 N HCl (100 mL) and water (50 mL). The organic phase was separated, dried with sodium sulfate, filtered, and concentrated to afford a gray solid, which was purified (PE/EA = 1/1) to afford compound **8** (1.2 g, yield of 75% with purity of >95% by HPLC).

7-Amino-2-(4′-(dimethylamino)phenyl)-8-nitro-4*H*-chromen-4-one (9). A mixture of 3-acetamido-6-acetyl-2-nitrophenyl 4-(dimethylamino)benzoate (compound **8**, 2 g) and potassium hydroxide (8 g) in pyridine (20 mL) was heated to 60 °C for 1 h and then poured into icy 1 N HCl (100 mL). The yellow solid was collected and dissolved in acetic acid (20 mL) and concentrated sulfuric acid. The resulting mixture was heated to 110 °C for 30 min. The mixture was cooled to room temperature and then poured into saturated sodium carbonate. The yellow solid was filtered and dried in vacuo to afford 7-amino-2-(4-(dimethylamino)phenyl)-8-nitro-4*H*-chromen-4-one (compound **9** with R = dimethylamino) (1.5 g, yield of 89% with purity of >95% by HPLC).

7,8-Diamino-2-(4′-(dimethylamino)phenyl)-4*H*-chromen-4-one Hydrochloride (10). A solution of 7-amino-2-(4-(dimethylamino)phenyl)-8-nitro-4*H*-chromen-4-one (compound **9**, 900 mg, 2.77 mmol) and 10% Pd/C (450 mg) in methanol (9 mL) and concentrated hydrochloride (aqueous, 9 mL) was stirred in an atmosphere of hydrogen overnight. The solid was filtered and the filtrate was evaporated at reduced pressure to afford 7,8-diamino-2-(4′-(dimethylamino)phenyl)-4*H*-chromen-4-one hydrochloride (compound **10**) as a light yellow solid (810 mg, yield of 88% with purity of >95% by HPLC).

8-(4′-(Dimethylamino)phenyl)chromeno[7,8-*d*]imidazol-6(1*H*)-one (11). A solution of 7,8-diamino-2-(4′-(dimethylamino)-phenyl)-4*H*-chromen-4-one hydrochloride (compound **10**, 500 mg) in HCO_2H (5 mL) was heated to reflux for 1 h. The volatiles were evaporated at reduced pressure, and the residue was partitioned between EA/isopropanol = 20/1 (50 mL) and saturated sodium carbonate (25 mL). The organic phase was separated, dried with sodium sulfate, filtered, and concentrated to afford a yellow solid, which was recrystallized from EA (25 mL) to afford a light yellow solid (compound **11** with R= dimethylamino, 111 mg, yield of 24%). ^1H NMR (300 MHz, DMSO-d_6) δ 8.46 (m,1H), 10.09 (br s, 1H), 8.01 (m, 2H), 7.82 (m, 1H), 7.61 (m, 2H), 6.84–6.88 (m, 3H). MS-ESI calculated, 305; found, 306(M + H)$^+$. HPLC: 99.23%

8-(4′-(Pyrrolidin-1-yl)phenyl)chromeno[7,8-*d*]imidazol-6(1*H*)-one (12 and 13). To a solution of compound *N*-(4-acetyl-3-hydroxy-2-nitrophenyl)acetamide (compound **6**, 700 mg, 2.94 mmol) in dry DCM (dichloromethane,10 mL) was added DIPEA (*N*,*N*-diisopropylethylamine, 0.8 mL) followed by compound **7** 4-(pyrrolidin-1-yl)benzoyl chloride (950 mg) at 0 °C, and the resulting mixture was stirred at room temperature overnight. The mixture was quenched with water and extracted with dichloromethane. The combined extracts were washed with water and brine and dried over Na_2SO_4. The mixture was concentrated and purified by silica gel (PE to PE/EA = 10:1 to 7:1 to 5:1 to 3:1) to give the coupled ester compound as an orange solid (750 mg), which was then followed by similar procedures as described for compound **11**. After cyclization with KOH/pyridine, followed by H_2SO_4/AcOH reflux, the nitro group in the intermediate was reduced with Fe (300 mg, 5.36 mmol) and NH_4Cl (154 mg, 2.85 mmol) to yield the reduced 7,8-diamino compound **10** with R = pyrrolidin-1-yl. A mixture of compound 7,8-diamino-2-(4′-(*N*-pyrrolidino)phenyl)-4*H*-chromen-4-one hydrochloride (1.1 g) in HCOOH (10 mL) was refluxed for 2 h. TLC showed the reaction was over. Combined with other batches, the mixture was basified to pH ≈ 8 by 1 N NaOH. The mixture was then concentrated and purified by silica gel (dichloromethane to dichloromethane/MeOH = 100:1 to 50:1 to 20:1) to give a mixture of compound **12** and 2-methylated compound **13** (80 mg), which was purified by pre-HPLC to give compound **12** as an orange solid (50 mg, confirmed by ^1H NMR) and compound **13** as dark-orange solid (25 mg, confirmed by ^1H NMR). For **12**: ^1H NMR (400 MHz, CD_3OD) δ 8.81 (s, 1H), 8.04 (m, 3H), 7.68 (d, J = 8.8 Hz, 1H), 6.78 (s, 1H), 6.66 (d, J = 8.8 Hz, 2H), 3.37 (m, 4H), 2.07 (m, 4H). HPLC: 96%. MS-ESI calculated, 331.4; found, 332.1 (M + 1)$^+$. For **13**: ^1H NMR (400 MHz,

CD3OD): δ 8.09 (d, J = 8.4 Hz, 1H), 8.01(d, J = 8.4 Hz, 2H), 7.64 (d, J=8.4 Hz, 1H), 6.78 (s, 1H), 6.69(d, J = 8.8 Hz, 2H), 3.41 (m, 4H), 2.92 (s, 3H), 2.10 (m, 4H); HPLC: 94%; MS-ESI: calculated: 345.4; found: 345.9 $(M + 1)^+$.

8-(4′-(Pyrrolidino)phenyl)chromeno[7,8-*d*]indoloyl-6(1*H*)-one (23). Methyl 2-Methoxy-4-methylbenzoate (15). A mixture of compound **14** (10 g, 65.73 mmol), CH_3I (37.32 g, 262.9 mmol), and K_2CO_3 (45.4 g, 329 mmol) in dry DMF (100 mL) was stirred at room temperature overnight. TLC showed the reaction was over. The mixture was filtered, and the filtrate was concentrated. The residue was diluted with EA, washed with water and brine, and dried over Na_2SO_4. The mixture was concentrated to give compound **15** as a yellow oil (with purity of >95% by HPLC, 12 g, confirmed by ^{1}H NMR, 100% yield). ^{1}H NMR (400 MHz, $CDCl_3$): δ 7.71 (d, J = 8.4 Hz, 1H), 6.78 (m, 2H), 3.89 (s, 3H), 3.87 (s, 3H), 2.38 (s, 3H).

Methyl 2-Methoxy-4,5-dimethylbenzoate (16). To a solution of compound **15** (10.0 g, 55.5 mmol) in dry DMF (80 mL) was added NCS (8.15 g, 61 mmol) in portions, and the resulting mixture was stirred at room temperature overnight. The mixture was concentrated, and the residue was dissolved in EA, washed with water and brine, and dried over Na_2SO_4. The mixture was concentrated to give compound **16** as a yellow solid (with purity of >95% by HPLC, 11.0 g, confirmed by ^{1}H NMR). ^{1}H NMR (400 MHz, $CDCl_3$): δ 7.78 (s, 1H), 6.83 (s, 1H), 3.88 (m, 6H), 2.39 (s, 3H).

Methyl 2-Methoxy-4,5-dimethyl-3-nitrobenzoate (17). To a solution of compound **16** (5 g, 23.3 mmol) in concentrated H_2SO_4 (23 mL) at 0 °C was added HNO_3 (2.3 mL) in portions, and the resulting mixture was stirred at 0 °C for 2 h. TLC showed the reaction was over. The mixture was poured into ice and extracted with Et_2O. The combined extracts were washed with water and brine, dried, and concentrated to give compound **17** as a yellow oil (with purity of >95%, 4.5 g, confirmed by ^{1}H NMR). ^{1}H NMR (400 MHz, $CDCl_3$): δ 7.99 (s, 1H), 3.92 (m, 6H), 2.33 (s, 3H).

(*E*)-Methyl 4-(2-(Dimethylamino)vinyl)-2-methoxy-5-methyl-3-nitrobenzoate (18). A mixture of compound **17** (2.6 g, 10 mmol) in dry DMF(10 mL) was treated with dimethylformamide−dimethylacetal (DMF−DMA) (3.58 g, 30 mmol), and the mixture was stirred at 120 °C overnight. TLC showed the reaction was over. The mixture was cooled and concentrated, and the residue was dissolved in EA, washed with water and brine, and dried over Na_2SO_4. The mixture was concentrated to give a crude as a brown semisolid (compound **18** with purity of >95%, 3 g, used for the next step without further purification).

Methyl 7-Methoxy-1*H*-indole-6-carboxylate (19). A mixture of compound **18** (3.1 g, 11.5 mmol) and $Pd(OH)_2$ (160 mg) in MeOH (20 mL) was stirred at room temperature under H_2 overnight. TLC showed the reaction was over. The mixture was filtered and concentrated and purified by silica gel (PE to PE/EA = 10:1 to 5:1) to give compound **19** as a white solid (with purity of >95%, 1.66 g, confirmed by ^{1}H NMR). ^{1}H NMR (400 MHz, $CDCl_3$): δ 8.61 (br s, 1H), 7.64 (d, J = 8.4 Hz, 1H), 7.38 (d, J = 8.4 Hz, 1H), 7.34 (m, 1H), 6.59 (m, 1H), 4.04 (s, 3H), 3.94 (s, 3H).

7-Methoxy-1*H*-indole-6-carboxylic Acid (20). A mixture of compound **19** (1.66 g, 8.09 mmol) and NaOH (1.62 g, 40 0.5 mmol) in MeOH (15 mL), THF (5 mL), and water (15 mL) was refluxed for 3 h. TLC showed the reaction was over. The mixture was cooled and concentrated, the residue was acidified to pH ≈ 2 by 2 N HCl, and the precipitate was collected by filtration and dried to give compound **20** as an off-white solid (with purity of >95% by HPLC, 980 mg, confirmed by ^{1}H NMR). ^{1}H NMR (400 MHz, DMSO-d_6): δ 12.41 (br s, 1H), 11.59 (s, 1H), 7.48 (s, 3H), 7.40 (d, J = 8.0 Hz, 1H), 7.31 (d, J = 8.4 Hz, 1H), 6.50 (s, 1H), 3.92 (s, 3H).

7-Methoxy-1*H*-indole-6-carbonyl Chloride (21). To a mixture of compound **20** (100 mg, 0.523 mmol) in dry THF (5 mL) was added DMF followed by $(COCl)_2$ (77 mg, 0.61 mmol) at 0 °C, and the resulting mixture was stirred at 0 °C for 1 h. TLC showed the reaction was almost over. The mixture was concentrated to give compound **21** as a yellow solid, which was used for the next step without further purification.

2-(4-(Pyrrolidin-1-yl)phenyl)pyrano[3,2-*g*]indol-4(9*H*)-one (23). To a solution of compound 4′-*N*-pyrrolidinobenzoyl methyl ketone (154 mg, 0.813 mmol) in dry THF(10 mL) at −20 °C was added LiHMDS (2 mL, 2 mmol), and the mixture was stirred at −20 °C for 1 h. Compound **21** 7-methoxy-6-indoloyl chloride (200 mg, 0.976 mmol) with $(COCl)_2$) in dry THF was added, and the mixture was stirred at −20 °C for 1 h and then at room temperature overnight. TLC and LC−MS showed the desired product was found. The mixture was quenched with aqueous NH_4Cl and extracted with EA, and the combined extracts were washed with water and brine and dried over Na_2SO_4. The mixture was concentrated and purified by silica gel (PE to PE/EA = 5:1 to 2:1) to give intermediate compound **22**, which was refluxed in HBr (48%, 6 mL) for 3 h. TLC showed the reaction was over. The mixture was combined with other batches and cooled to room temperature. Water was added and the mixture was basified to pH ≈ 8 by NaOH (1 N) and concentrated and purified by silica gel (dichloromethane to dichloromethane/MeOH = 20:1 to 10:1) to give crude compound **23** as a brown solid. This crude product was purified by pre-HPLC to give compound **23** as a brown solid. ^{1}H NMR (400 MHz, DMSO-d_6): δ 12.40 (br s, 1H), 8.16 (d, J = 8.8 Hz, 2H), 7.70 (s, 1H), 7.57 (s, 2H), 6.80 (s, 1H), 6.68 (m, 3H), 3.36 (m, 4H), 2.00 (m, 4H). HPLC: 99%. MS-ESI calculated, 330.4; found, 331.1 $(M + 1)^+$.

Phospho-Akt S473 ELISA. PathScan phospho-Akt1 (Ser473) Sandwich ELISA kit was purchased from Cell Signaling (catalog no. 7160). A 100 μL sample in sample diluent (supplied in the kit) was added to each well and incubated overnight at 4 °C. After 4× wash with 200 μL of wash buffer (supplied in the kit), 100 μL/well detection antibody was added and the mixture was incubated for 1 h at 37 °C. After 4× wash, 100 μL of HRP-linked secondary antibody (supplied in the kit) was added, and the mixture was incubated for 30 min at 37 °C. After a final wash, 100 μL of TMB substrate was added to each well and incubated for 10 min at 37 °C. The reaction was stopped by adding 100 μL/well stop solution. The values of each well were recorded using a microplate reader at 450 and 650 nm. The optical density was determined by the subtraction of the reading at 650 nm from the readings at 450 nm.

TrkB Agonists Drug Administration. Male C57BL/6 mice aged 2 months were orally administrated 4′-DMA-7,8-DHF derivatives in a single dose of 1 mg/kg for 4 h. The control mice were injected with saline. The mice were sacrificed, and brains were homogenized and ultracentrifuged. The supernatant (40 μg) was employed for SDS−PAGE and immunoblotting analysis with indicated antibodies, respectively. Male C57BL/6 mice aged 2 months were orally administrated compound **32** or **11** at a dose of 5 mg kg^{-1} day^{-1} each and compound **13** or **23** at a dose of 2.5 mg kg^{-1} day^{-1} each for 21 days. BrdU (100 mg/kg) was ip injected 2 h before the TrkB agonist treated animals were sacrificed and the hippocampal section lysates were analyzed by immunoblotting with p-TrkB and total TrkB antibodies, p-AKT ELISA.

Immunohistochemistry Staining. Brain tissues were fixed in 4% paraformaldehyde overnight followed by paraffin embedding. Sections of 6 μm were cut. For immunohistochemical staining, brain sections were deparaffinized in xylene and rehydrated in graded alcohols. Endogenous peroxidase activity was blocked by 3% hydrogen peroxide for 5 min, and all slides were boiled in 10 mM sodium citrate buffer (pH 6.0) for 10 min. Phosphorylated TrkB 816 and TrkB were detected using specific antibodies. Paraffin sections were deparaffinized in xylene and rehydrated in gradient ethanol solution. Samples were boiled in 10 mM sodium citrate buffer for 20 min for antigen retrieval purpose. Brain sections were incubated with anti-TrkB (BD Biosciences, San Jose, CA), 1:50, p-TrkB, 1:300 dilution. Secondary antibody was applied using anti-rabbit-Alexa 594 (red) and anti-mouse-fluorescein isothiocyanate (FITC) (green). DAPI (blue) was used for nuclear staining.

Forced Swim Test. Adult male mice (2−3 months old) were randomly submitted to a forced swim test without a preswim. Saline and TrkB agonists were orally administrated by gavage for 21 days. The mice were allowed to adapt to the test room for 2 days. The mice were placed in a clear glass cylinder with a diameter of 16 cm, half-

dx.doi.org/10.1021/jm301099x | J. Med. Chem. 2012, 55, 8524−8537

filled with clear water at 24 °C (water depth of 14 cm did not allow the mice to reach the bottom of the cylinder) for a total of 6 min, and immobility was recorded during the last 4 min by an investigator blind to the treatment.

Tail Suspension Test. Mice were individually suspended by the tail to a horizontal ring stand bar 30 cm above the floor using adhesive tape for 6 min and videotaped. Latency to immobility and time spent immobile were scored for each mouse. Following the test, mice were returned to their home cage. Immobility scores were compared by unpaired *t* test.

Locomotor Activity. Locomotor activity was assessed using an automated system (San Diego Instruments, La Jolla, CA, U.S.) with photobeams that recorded ambulations (consecutive beam breaks). Drug-treated mice were placed in the locomotor chambers, and their activity was recorded for 2 h at 30 min intervals.

Neurogenesis Analysis in TrkB-Agonists-Treated Hippocampus. Adult male mice (2−3 months old) were orally administrated with saline, **13**, and **23** (2.5 mg/kg) for 21 days. Then BrdU (100 mg/kg) was ip injected. In 2 h, the mice were perfused with 4% paraformaldehyde. Immunohistochemical staining was performed on formalin-fixed paraffin embedded sections. Sections from brain were cut, deparaffinized in xylene, and rehydrated in graded alcohols. The slides were boiled in 10 mM citric acid (pH 6.0) for 10 min, followed by an incubation in 2 N HCl for 10 min in room temperature. The slides were then permeabilized and blocked with 1% BSA in 0.2% PBS Tween-20 (PBST). The incorporated BrdU was stained using anti-BrdU-FITC (Abcam, U.S.) at 4 °C for 16 h. After three times of washing in PBS, the cells were then stained with DAPI for another 10 min at room temperature. The slides were finally mounted with AquaMount (Lerner Laboratories, U.S.) containing 0.01% 1,4-diazobicyclo(2,2,2)octane and examined under a fluorescence microscope.

Micronucleus Assay. The cells treated with 7,8-DHF derivatives at 50 μM for 24 h were washed with PBS, incubated in mild hypotonic solution (0.075 M KCL/0.9% NaCl, 1:19) for 10 min at 37 °C, fixed with methanol−glacial acetic acid (3:1) for 15 min at 37 °C, rinsed with distilled water, and air-dried. Fixed cells were stained with DAPI (2 μg/mL) for 30 min in the dark at room temperature. Cells were rinsed with PBS and distilled water and mounted with Fluoromount-G (Southern Biotech). Micronuclei were identified based on the criteria specified by Miller at al.[27] One-thousand cells per treatment were analyzed using the fluorescence microscope. Data are the mean ± SEM of three independent experiments.

Single Cell Gel Electrophoresis (SCGE, the Comet Assay). The treated and control HepG2 cells embedded in 0.75% LMP (low melting point) agarose and spread on a base layer of 1% NMP (normal melting point) agarose in PBS buffer were placed in a lysis solution (2.5 M NaCl, 200 mM Na_2EDTA, 10 mM Tris-HCl, pH 10, and 1% Triton X-100) at 4 °C for 2 h. Slides were transferred to an electrophoresis box and immersed in an alkaline solution (300 mM NaOH, 1 mM Na_2EDTA, pH > 13). After a 40 min unwinding time, a voltage of 25 V (300 mA) was applied for 30 min at 4 °C. Slides were neutralized with 3 × 5 min washes with Tris-HCl (0.4 M, pH 7.4) and stained with ethidium bromide (EtBr, 10 μg/mL). EtBr stained nucleotides were examined with fluorescence microscope. Total cell numbers in a field (>100) were counted, and the number of nucleoids exhibiting comet tail formation was identified.[22,28] Results were quantified as the number of comet nuclei out of the total number of nuclei observed from three independent experiments.

In Vitro ADMET and in Vivo Pharmacokinetic Studies. Mice of 20−30 g at age of 6−8 weeks were administrated with the indicated compounds iv or orally. At different time points (3, 10, 30, 60, 120, 240, 360, and 480 min), blood aliquots (300−400 mL) were collected in tubes coated with lithium heparin, mixed gently, then kept on ice, and centrifuged at 2500*g* for 15 min at 4 °C within 1 h of collection. The plasma was then harvested and kept frozen at −20 °C until further processing. For each time point, 3 mice/group were employed. The plasma samples were analyzed by HPLC. The in vitro ADMET assays were conducted in Apredica, Inc. The experimental conditions for the ADMET are available at www.apredica.com. The standard and control compounds for ADMET assays are included in Supporting Information Tables 1−4.

Homology Modeling and Docking of 7,8-DHF to TrkB ECD. A structure-guided sequence alignment between human TrkA ECD and human TrkB ECD was edited to accommodate the short deletions/insertions at the tips of the connecting loops between secondary structural elements. A monomeric structure of TrkA was selected from the crystal structure of the TrkA-nerve growth factor complex (PDB code 2IFG)[29] as the template. Comparative modeling was carried out with the MODELLER program by satisfaction of spatial restraints.[30] Docking of 7,8-DHF to the modeled TrkB ECD structure was carried out with MEDock based on a maximum entropy optimization algorithm.[31] The top five probable solutions resulting from random seed searches, with the lowest docked energies ranging from −9.3 to −8.7 kcal/mol, were selected for graphical analysis.

■ ASSOCIATED CONTENT

Ⓢ Supporting Information

Two figures showing 7,8-DHF metabolism and molecular modeling; four tables listing the positive controls in the ADMET profiling. This material is available free of charge via the Internet at http://pubs.acs.org.

■ AUTHOR INFORMATION

Corresponding Author

*Phone: 404-712-2814. E-mail: kye@emory.edu.

Notes

The authors declare no competing financial interest.

■ ACKNOWLEDGMENTS

This work is supported by grant from NIDCD, National Institutes of Health (Grant RO1 DC010204), to K.Y. The authors thank Andrei Halavaty for the help in molecular modeling. The authors are thankful to Dr. Obianyo at the Ye laboratory for proofreading of the manuscript.

■ ABBREVIATION USED

7,8-DHF, 7,8-dihydroxyflavone; 4′-DMA-7,8-DHF, 4′-dimethylamino-7,8-dihydroxyflavone; ECD, extracellular domain; BDNF, brain-derived neurotrophic factor; FITC, fluorescein isothiocyanate; NGF, nerve growth factor; DAPI, 4′,6-diamidino-2-phenylindole; TrkB, tropomyosin-related kinase B; NT-3, neurotrophic factor 3; MeCP2, methyl CpG binding protein 2; FST, forced swim test; TST, tail suspension test; COMT, catechol methyltransferase; LDH, lactate dehydrogenase

■ REFERENCES

(1) Nibuya, M.; Morinobu, S.; Duman, R. S. Regulation of BDNF and trkB mRNA in rat brain by chronic electroconvulsive seizure and antidepressant drug treatments. *J. Neurosci.* **1995**, *15*, 7539−7547.

(2) Saarelainen, T.; Hendolin, P.; Lucas, G.; Koponen, E.; Sairanen, M.; MacDonald, E.; Agerman, K.; Haapasalo, A.; Nawa, H.; Aloyz, R.; Ernfors, P.; Castren, E. Activation of the TrkB neurotrophin receptor is induced by antidepressant drugs and is required for antidepressant-induced behavioral effects. *J. Neurosci.* **2003**, *23*, 349−357.

(3) Monteggia, L. M.; Barrot, M.; Powell, C. M.; Berton, O.; Galanis, V.; Gemelli, T.; Meuth, S.; Nagy, A.; Greene, R. W.; Nestler, E. J. Essential role of brain-derived neurotrophic factor in adult hippocampal function. *Proc. Natl. Acad. Sci. U.S.A.* **2004**, *101*, 10827−10832.

(4) Li, Y.; Luikart, B. W.; Birnbaum, S.; Chen, J.; Kwon, C. H.; Kernie, S. G.; Bassel-Duby, R.; Parada, L. F. TrkB regulates hippocampal neurogenesis and governs sensitivity to antidepressive treatment. *Neuron* **2008**, *59*, 399−412.

(5) Sahay, A.; Hen, R. Adult hippocampal neurogenesis in depression. *Nat. Neurosci.* **2007**, *10*, 1110−1115.
(6) Schmidt, H. D.; Duman, R. S. The role of neurotrophic factors in adult hippocampal neurogenesis, antidepressant treatments and animal models of depressive-like behavior. *Behav. Pharmacol.* **2007**, *18*, 391−418.
(7) Banasr, M.; Duman, R. S. Regulation of neurogenesis and gliogenesis by stress and antidepressant treatment. *CNS Neurol. Disord.: Drug Targets* **2007**, *6*, 311−320.
(8) Lindsay, R. M. Role of neurotrophins and trk receptors in the development and maintenance of sensory neurons: an overview. *Philos. Trans. R. Soc. London, Ser. B* **1996**, *351*, 365−373.
(9) Siegel, G. J.; Chauhan, N. B. Neurotrophic factors in Alzheimer's and Parkinson's disease brain. *Brain Res. Rev.* **2000**, *33*, 199−227.
(10) Jang, S. W.; Liu, X.; Yepes, M.; Shepherd, K. R.; Miller, G. W.; Liu, Y.; Wilson, W. D.; Xiao, G.; Blanchi, B.; Sun, Y. E.; Ye, K. A selective TrkB agonist with potent neurotrophic activities by 7,8-DHF. *Proc. Natl. Acad. Sci. U.S.A.* **2010**, *107*, 2687−2692.
(11) Jang, S. W.; Liu, X.; Chan, C. B.; France, S. A.; Sayeed, I.; Tang, W.; Lin, X.; Xiao, G.; Andero, R.; Chang, Q.; Ressler, K. J.; Ye, K. Deoxygedunin, a natural product with potent neurotrophic activity in mice. *PLoS One* **2010**, *5*, e11528.
(12) Liu, X.; Chan, C. B.; Jang, S. W.; Pradoldej, S.; Huang, J.; He, K.; Phun, L. H.; France, S.; Xiao, G.; Jia, Y.; Luo, H. R.; Ye, K. A synthetic 7,8-DHF derivative promotes neurogenesis and exhibits potent antidepressant effect. *J. Med. Chem.* **2010**, *53*, 8274−8286.
(13) Devi, L.; Ohno, M. 7,8-DHF, a small-molecule TrkB agonist, reverses memory deficits and BACE1 elevation in a mouse model of Alzheimer's disease. *Neuropsychopharmacology* **2012**, *37*, 434−444.
(14) Blugeot, A.; Rivat, C.; Bouvier, E.; Molet, J.; Mouchard, A.; Zeau, B.; Bernard, C.; Benoliel, J. J.; Becker, C. Vulnerability to depression: from brain neuroplasticity to identification of biomarkers. *J. Neurosci.* **2011**, *31*, 12889−12899.
(15) Zeng, Y.; Tan, M.; Kohyama, J.; Sneddon, M.; Watson, J. B.; Sun, Y. E.; Xie, C. W. Epigenetic enhancement of BDNF signaling rescues synaptic plasticity in aging. *J. Neurosci.* **2011**, *31*, 17800−17810.
(16) Johnson, R. A.; Lam, M.; Punzo, A. M.; Li, H.; Lin, B. R.; Ye, K.; Mitchell, G. S.; Chang, Q. 7,8-DHF exhibits therapeutic efficacy in a mouse model of Rett syndrome. *J. Appl. Physiol.* **2012**, *112*, 704−710.
(17) LeWitt, P. A. Subcutaneously administered apomorphine: pharmacokinetics and metabolism. *Neurology* **2004**, *62*, S8−S11.
(18) Di Stefano, A.; Sozio, P.; Cerasa, L. S.; Iannitelli, A. L-Dopa prodrugs: an overview of trends for improving Parkinson's disease treatment. *Curr. Pharm. Des.* **2011**, *17*, 3482−3493.
(19) Cryan, J. F.; Markou, A.; Lucki, I. Assessing antidepressant activity in rodents: recent developments and future needs. *Trends Pharmacol. Sci.* **2002**, *23*, 238−245.
(20) Petit-Demouliere, B.; Chenu, F.; Bourin, M. Forced swimming test in mice: a review of antidepressant activity. *Psychopharmacology (Berlin, Ger.)* **2005**, *177*, 245−255.
(21) Cryan, J. F.; Mombereau, C.; Vassout, A. The tail suspension test as a model for assessing antidepressant activity: review of pharmacological and genetic studies in mice. *Neurosci. Biobehav. Rev.* **2005**, *29*, 571−625.
(22) Kozics, K.; Valovicova, Z.; Slamenova, D. Structure of flavonoids influences the degree inhibition of benzo(*a*)pyrene-induced DNA damage and micronuclei in HepG2 cells. *Neoplasma* **2011**, *58*, 516−524.
(23) Wang, J.; Urban, L.; Bojanic, D. Maximising use of in vitro ADMET tools to predict in vivo bioavailability and safety. *Expert Opin. Drug Metab. Toxicol.* **2007**, *3*, 641−665.
(24) Sanguinetti, M. C.; Tristani-Firouzi, M. hERG potassium channels and cardiac arrhythmia. *Nature* **2006**, *440*, 463−469.
(25) Redfern, W. S.; Carlsson, L.; Davis, A. S.; Lynch, W. G.; MacKenzie, I.; Palethorpe, S.; Siegl, P. K.; Strang, I.; Sullivan, A. T.; Wallis, R.; Camm, A. J.; Hammond, T. G. Relationships between preclinical cardiac electrophysiology, clinical QT interval prolongation and torsade de pointes for a broad range of drugs: evidence for a provisional safety margin in drug development. *Cardiovasc. Res.* **2003**, *58*, 32−45.
(26) Goldkind, L.; Laine, L. A systematic review of NSAIDs withdrawn from the market due to hepatotoxicity: lessons learned from the bromfenac experience. *Pharmacoepidemiol. Drug Saf.* **2006**, *15*, 213−220.
(27) Miller, B. M.; Pujadas, E.; Gocke, E. Evaluation of the micronucleus test in vitro using Chinese hamster cells: results of four chemicals weakly positive in the in vivo micronucleus test. *Environ. Mol. Mutagen.* **1995**, *26*, 240−247.
(28) Kivovich, V.; Gilbert, L.; Vuento, M.; Naides, S. J. The putative metal coordination motif in the endonuclease domain of human parvovirus B19 NS1 is critical for NS1 induced S phase arrest and DNA damage. *Int. J. Biol. Sci.* **2012**, *8*, 79−92.
(29) Wehrman, T.; He, X.; Raab, B.; Dukipatti, A.; Blau, H.; Garcia, K. C. Structural and mechanistic insights into nerve growth factor interactions with the TrkA and p75 receptors. *Neuron* **2007**, *53*, 25−38.
(30) Eswar, N.; Webb, B.; Marti-Renom, M. A.; Madhusudhan, M. S.; Eramian, D.; Shen, M. Y.; Pieper, U.; Sali, A. Comparative Protein Structure Modeling Using Modeller. In *Current Protocols in Bioinformatics*; Wiley: New York, 2006; Chapter 5, Unit 5 6.
(31) Chang, D. T.; Oyang, Y. J.; Lin, J. H. MEDock: a Web server for efficient prediction of ligand binding sites based on a novel optimization algorithm. *Nucleic Acids Res.* **2005**, *33*, W233−W238.